

DESIGN OF CIRCULARLY POLARIZED OMNIDIRECTIONAL BIFILAR HELIX ANTENNAS WITH OPTIMUM WIDE AXIAL RATIO BEAMWIDTH

Jawad Yousaf*, Muhammad Amin, and Sana Iqbal

Department of Electrical Engineering, Institute of Space Technology, Islamabad Highway, Islamabad 44000, Pakistan

Abstract—In this paper, design and analysis of omnidirectional single feed circularly polarized, wide axial ratio beamwidth resonant side-fed bifilar helix antennas that do not require a ground plane is presented. The simulation and measurement results show that side-fed helix antennas of various radii gives near perfect circular polarization (CP) almost over the whole sphere except at and around nulls, at a certain turn angle by properly proportioning the area of loop (A) with the product of pitch (ρ) and radianlength (l) of helix. Helix antennas with smaller radii give axial ratio (AR) close to one at higher values of turn angle with lower value of resonant input impedances but CP is less sensitive to inaccuracy in turn angle. However helix antennas with larger radii results in AR close to one at lower values of turn angle and provides better values of input resistance but its AR is more sensitive to variations in turn angle. The simulated results show that the polarization solid angle beamwidth (for $AR \leq 3$ dB) varies from 3.96π to 4π steradian. The gain and 3 dB beamwidth of the antennas are 2 dBi and 90° respectively. The polarization bandwidth varies from 34% to 65%. The simulated results are verified by experimental measurements.

1. INTRODUCTION

Omnidirectional antennas are very useful for communication where relative direction between transmit and receive antenna is not known or changes continuously and randomly [1–3]. Circularly Polarized (CP) omnidirectional antennas increase the reliability of communication system [2, 4–7] because depolarization of electromagnetic (EM) waves

Received 21 February 2013, Accepted 11 April 2013, Scheduled 17 April 2013

* Corresponding author: Jawad Yousaf (jawad.yousaf@yahoo.com).

due to scattering and diffraction does not deteriorate the reception in circular polarization as adversely as in linear polarization [8, 9]. CP omnidirectional antennas provide better performance in multipath environment [10–12], because a reflected CP wave changes its sense of rotation [13]. The impedance of CP antennas because of energy reflected from metallic objects (e.g., when used as a feed) also does not change [14]. In free space propagation, a polarization misaligned CP antenna will give a maximum of 3 dB loss. Most omnidirectional antennas are linearly polarized or dual linearly polarized [3, 15–18], of which many configurations require ground plane [9–21]. Similarly CP omnidirectional antennas are of two categories, one which require ground plane (slot type or monopole type) [2, 5, 22–25] and other which do not require ground plane (frequency independent antennas, Quadrifilar Helix Antenna (QHA) and orthogonally oriented vee dipoles) [26–29]. CP antennas which do not require ground plane are attractive for application where proper ground plane is not available, or ground plane is not suitable for use, such as high speed aerodynamic surfaces, Unmanned Aerial Vehicles (UAVs), mini UAVs made of composite material, and small handheld devices which cannot provide ground plane for monopole operation or devices made of non-metallic material [6].

In this paper, we present the design and analysis of CP omnidirectional helix antennas [30] which do not require ground plane based on the equation described in [31] by Wheeler. The helix antenna provides AR of nearly unity over the whole 4π steradian solid angle except at and around nulls, and to the best knowledge of authors this antenna provides maximum solid angle polarization beamwidth (for $AR \leq 3$ dB) in the class of omnidirectional resonant antennas in elevation plane at any azimuth angle. The design of various CP helix antennas is validated by Numerical Electromagnetic Code (NEC) [32] simulations and measurements. The CP omnidirectional antenna is a resonant Side-fed Bifilar Helix Antenna (SFBHA) where the feed is on one of the helical arms of the helix such that the current in both helical arms is in the same direction like the current in two arms of the folded dipole antenna. The helix effectively becomes a combination of a dipole and a loop antenna [Figure 1] [31]. The original field responsible for radiation in case of dipole is electric field and for the loop is magnetic field and these two fields are at quadrature in time-phase so are the two radiated fields. Since the radiated electric fields from dipole and a loop are also spatially at right angle to each other, CP is achieved if the radiated electric fields are of same magnitude [14]. The reported SFBHAs, to the best knowledge of authors, are the lowest profile CP antennas without ground plane with their heights range from

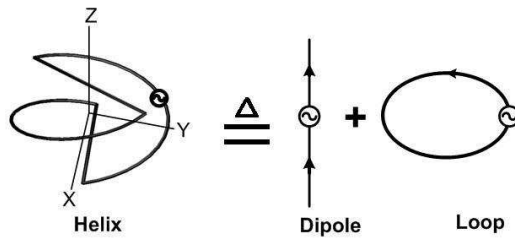


Figure 1. Basic helix antenna structure.

0.03λ to 0.1λ. The previously reported CP antennas include frequency independent antennas of height ≥ 2λ [27], orthogonally oriented vee dipoles of height ≥ 0.5λ [9] and dual polarized omnidirectional antenna of height 0.87λ [33]. The proposed antennas can be scaled for any frequency as long as its size remains reasonable. The possible use of these proposed antennas include various communication applications developed in ISM band, personal communication handsets, cordless phones, various applications of short range devices such as Wi-Fi, bluetooth etc. [6].

2. HELIX ANTENNA AND CIRCULAR POLARIZATION

CP waves can be generated by a helix antenna by properly proportioning the area (*A*) of the loop that has a radius *r* and is formed when helix is given certain turn angle, with the product of pitch (*ρ*) and radianlength (*l* = λ/2π) of the helix at a specific frequency as given in [31]

$$A = \rho l \tag{1}$$

Equation (1) is derived from the fact that the amplitude of electric and magnetic fields of a loop *E_m*, *H_m* should equal that of dipole *E_o*, *H_o* for CP [14], i.e.,

$$\frac{E_m}{E_o} = 1 = \frac{\eta}{E_o/H_o} = \eta \frac{H_o}{E_o} = \eta \frac{H_m}{E_o} \tag{2}$$

The ratio *H_m/E_o* will be proportional to their relative magnetic and electric fluxes of dipole and loop respectively which in turn equals the ratio of the magnetic moment of loop and electric moment of the dipole

$$\frac{B_m}{D_o} = \frac{\mu H_m}{\epsilon E_o} = \frac{\mu I A}{I \rho / j \omega} = \eta \tag{3}$$

The corresponding electric fields in Equation (3) are in phase quadrature as indicated by the differential operator *jω* which results in

near perfect CP when additionally the magnitudes of the two fields are equal (Equation (2)) [14, 34, 35]. It can be shown that Equation (1) can be derived from Equation (3) [31].

Substituting pitch of helical antenna ($\rho = \frac{l}{2}$) equal to dipole length and taking its product with radianlength ($l = \lambda/2\pi$) will produce the CP if the CP conditions are fulfilled by equating it to the area of loop antenna of radius a .

$$A = \text{pitch} \times \text{radianlength} = \left(\frac{l}{2}\right) \left(\frac{\lambda}{2\pi}\right) = \rho l \quad (4)$$

$$a = \frac{\sqrt{l\lambda}}{2\pi} \quad (5)$$

The above expression (1) can also be derived by equating the amplitudes of electric field components of small dipole and loop with implicit assumption of same current [14] in both the antennas. Equating magnitude of electric field of small dipole with that of loop [36] results

$$\begin{aligned} \overline{E}_{dipole} &= \overline{E}_{loop} \\ \eta \frac{kI_0 l e^{-jkr}}{8\pi r} \sin \theta &= \frac{kA\omega\mu I_0 l \sin \theta}{4\pi r} e^{-jkr} \\ \eta \frac{l}{2} &= A\omega\mu \end{aligned}$$

With $A = \pi a^2$, $\eta = \sqrt{\frac{\mu}{\epsilon}}$, above simplifies to the fundamental expression of (1) [31].

Alternatively, the same expression ($A = \rho l$) can be derived by equating radiation resistances of loop and dipole antennas [36] for identical current I_0 , i.e.,

$$\begin{aligned} Rr_{dipole} &= Rr_{loop} \\ 20 \times \pi^2 \left(\frac{l}{\lambda}\right)^2 &= 20 \times \pi^2 \left(\frac{C}{\lambda}\right)^4 \end{aligned} \quad (6)$$

Here l is the length of dipole and C the circumference of the loop. This too reduces to Equation (1).

3. DESIGN OF SIDE-FED BIFILAR HELIX ANTENNA

A SFBHA can be understood from a rectangular loop antenna which is fed from one of its vertical sides [Figure 2]. If the base (bottom radial section) of the rectangular loop is held fixed and it is rotated from the top radial section around its vertical axis, the vertical side

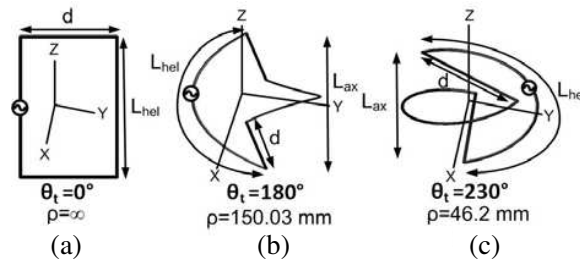


Figure 2. Helix antenna ($d = 55.2$ mm, $L_{hel} = 114.65$ mm) with various turn angles (a) $\theta_t = 0^\circ$, (b) $\theta_t = 180^\circ$, (c) $\theta_t = 230^\circ$.

of the rectangular loop (its length denoted by L_{hel} because it forms a helical path as it is given some turn angle) follows a path around an imaginary cylindrical surface of diameter d , called diameter of the helix [Figure 2]. The turn angle is proportional to the amount of rotation [28], e.g., the rotation through half cycle is equivalent to a turn angle of 180° [Figure 2(b)]. In the form of rectangular loop, the turn angle is zero while the pitch is infinite, and the axial length (L_{ax}) equals helical length (L_{hel}). As the turn angle increases the axial length and pitch of the helix decreases.

For a smaller d/L_{hel} ratio, the helix is to be rotated through higher turn angle to achieve CP, because for a smaller d/L_{hel} ratio, the area of loop formed by helix is smaller and to make it equal to the right hand side of Equation (1), its pitch has to be reduced, hence greater turn angle for smaller d/L_{hel} ratio and vice versa.

4. MODELING OF SIDE-FED BIFILAR HELIX ANTENNA

NEC is used for modeling and simulation of the SFBHAs. The perimeter length of the loop was chosen such that the helix with diameter 55.2 mm and 0° turn angle resonates around 1 GHz [30]. This results in total perimeter length of 340 mm with helical length equal to 114.65 mm [30]. The d/L_{hel} ratio for this configuration is 0.48 [30]. For helix with other configurations (different dias), the perimeter length was fixed, therefore d/L_{hel} was different for each helix of different diameter.

Helix antennas with six different diameters (d/L_{hel} ratios) are simulated. The radianlength for all was calculated using the corresponding resonant frequency, i.e., 860 MHz. For each case the turn angle was increased gradually. As the turn angle increases, axial

length (L_{ax}) decreases for a radius r according to the formula [30]

$$L_{ax} = \sqrt{L_{hel}^2 - \left(\frac{r\theta_t\pi}{180}\right)^2} \quad (7)$$

The turn angle increases from 0° to its maximum value, ideally determined by substituting $L_{ax} = 0$ in Equation (7) (for infinitely small radius of the wire)

$$\theta_t = \frac{L_{hel} \times 180}{r\pi} \quad (8)$$

Practically, the minimum axial length will depend on wire diameter, number of turns and spacing between the wires. For increasing turn angle, the pitch (ρ) and axial length (L_{ax}) decreases and hence the product ρl . For each d/L_{hel} , this is plotted in Figure 3, which illustrates the variation in ρl versus turn angle for different helix radii according to Equation (1). The area of each helix is represented as horizontal line in the same legend as the product ρl . The turn angle at which the product ρl intersects the corresponding horizontal line of the area A , is the value where near perfect CP (maximum value of AR) is achieved. Turn angle θ_{tCP} where maximum value of axial ratio is obtained is higher for smaller d/L_{hel} ratio (small helix radius) and is lower for larger d/L_{hel} ratio (large helix radius).

5. SIMULATION RESULTS

The simulation of the antenna starts with zero turn angle, i.e., a rectangular loop antenna which gives almost pure vertical field. As the turn angle increases the horizontal field starts to become significant. The vertical field is greater than the horizontal field up to a turn angle where near CP is achieved. When the turn angle is θ_{tCP} , the value of the horizontal field becomes approximately equal to the vertical field (as electric dipole moment $\times \eta =$ magnetic dipole moment, where η is the intrinsic impedance of the medium) and because the original source field responsible for radiation is electric and magnetic for dipole and loop antenna respectively, an almost pure CP is achieved.

In NEC simulation of helix for a particular d/L_{hel} ratio, if the frequency of operation is taken as frequency where imaginary component of input impedance is minimum, then this frequency varies for each turn angle and deviates from 860 MHz as has been assumed while plotting $A = \rho l$ in Figure 3. This resonant frequency where perfect CP is achieved is shown in Figure 4 for different diameters. Figure 4 shows that the input impedance of the antenna is proportional to the change in helix radius. Slight variation in resonance frequency

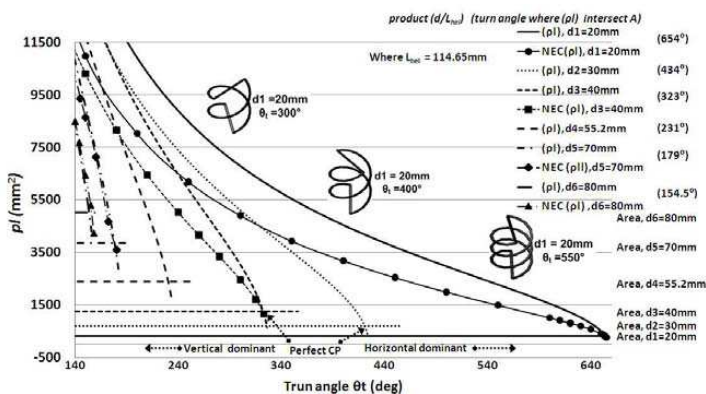


Figure 3. Turn angle θ_t vs. product of $\rho \times \frac{\lambda}{2\pi}$ (pitch \times radianlength).

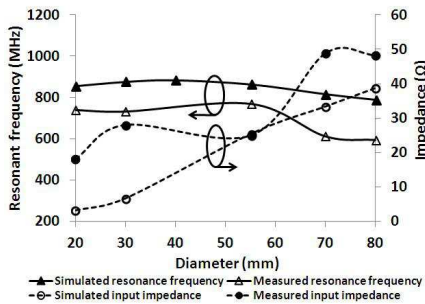


Figure 4. Resonant frequency and input impedance variations with diameter of helices at nearly perfect CP.

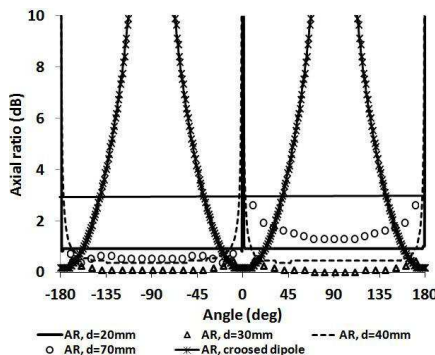


Figure 5. Simulated axial ratio variations for helices of different dias in elevation plane at their respective resonance frequencies.

produces negligible effect on the ρl product of Figure 3 because of minor variation in radianlength ($\lambda/2\pi$). If frequency of operation is assumed where imaginary part of the input impedance is minimum, than the radianlength ($\lambda/2\pi$) becomes different, that changes the product ρl . This has been simulated in NEC for four cases and graphs have been shown in Figure 3. It can be inferred that the deviation from theoretical graphs is larger for lower radius and minor for larger radius probably because of mutual coupling but the point where near-perfect CP is achieved, the deviation is negligible.

Figure 5 shows simulated axial ratio for various diameters of helices and cross dipole. The axial ratio of helices has fewer variations

for smaller radius and as the radius increases, axial ratio variation (within impedance bandwidth for $VSWR \leq 2$) increases but remains within $0 \text{ dB} \leq AR \leq 2 \text{ dB}$ covering almost whole elevation range except at and around nulls at any azimuth angle. For comparison in the case of crossed dipole, the $AR \leq 3 \text{ dB}$ only cover 60% of the elevation range.

These antennas provide AR better than 3 dB throughout the 4π steradian solid angle of the whole sphere except at and around the nulls ($AR \leq 3 \text{ dB}$ over solid angle of 0.04π steradian). Hence the 3 dB solid angle polarization beamwidth varies from 4π steradian to 3.96π steradian. These antennas therefore provides the best performance with respect to polarization solid angle beamwidth in the class of resonant omnidirectional antennas without ground plane. This is distinctive feature of SFBHAs in comparison to other CP antennas [37] where AR normally deteriorates as one moves away from the boresight (direction of maximum gain). For smaller radius ($r = 10 \text{ mm}$), the AR is identical on both sides of the elevation plane and on either side is constant over the whole elevation angle where as for larger radii (20 mm and above), the AR is not identical on both sides of the elevation plane and the difference is proportional to the radius of helix [Figure 5]. Furthermore the AR is also not constant on either side because of the difference in magnitudes between the vertical and horizontal fields and phase difference deviation from 90° . This is because of the path difference [38] (and hence the phase difference) from the two equivalent dipoles that give doughnut shaped radiation pattern, is higher for larger radius and lower for smaller radius.

The polarization bandwidth ($AR \leq 3 \text{ dB}$) of CP helix antenna varies from 34% ($d = 80 \text{ mm}$) to 65% ($d = 20 \text{ mm}$). In the azimuth plan the maximum gain variation is $< 0.64 \text{ dB}$, which is proportional to the radius of helix. The gain and beamwidth of the these helix antennas is nearly 2 dBi and 90° respectively. The computed/measured resonant frequencies vary from 855/740 MHz to 787/594 MHz respectively. The impedance bandwidth (for $VSWR \leq 2$) referenced to the input resonant resistance of the antennas varies from 0.8% to 4.2% and it is directly proportional to the d/L_{hel} ratios of the antennas [Figure 6].

6. COMPARISON OF SIMULATED AND MEASURED RESULTS

Helix antenna models are fabricated by grooving the helical paths on a cylinder equivalent to the diameter of the helix. The antennas are modeled in Pro-E software and the file of each model, is then converted into CNC machine readable format for manufacturing. These cylinders were fabricated from teflon material. Semi rigid coaxial cable (UT-

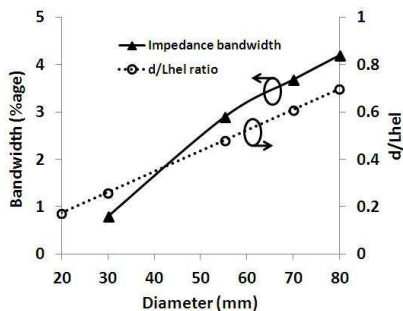


Figure 6. Impedance bandwidth and d/L_{hel} ratio variations of CP helix antennas with diameter.

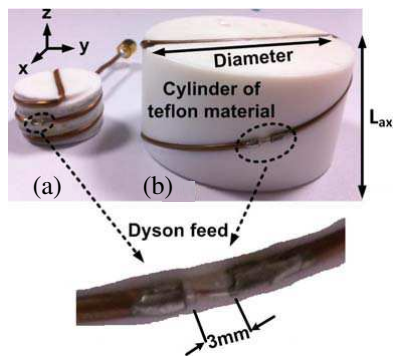


Figure 7. Photograph of manufactured models of CP helix antennas, (a) $d = 30$ mm, $L_{ax} = 15.39$ mm, (b) $d = 80$ mm, $L_{ax} = 38.89$ mm.

47-LL) of radius 1.1mm was used to form the helices of required turn angle, pitch and radius. An infinite balun type feed (dyson feed) [30] was used to excite the antennas [Figure 7]. The S -parameter measurements were carried out using Agilent E8362B vector network analyzer. The comparison of measured resonant frequencies and input impedances is shown in Figure 4. The measured and simulated input resistance values at resonance are in fairly good agreement; however, the measured resonant frequencies are on average 12% lower than the simulated one. This is because of the dielectric support used to maintain the precise geometry of the antennas.

The simulated and measured Return Loss (RL) of both antennas are depicted in Figure 8. The difference in magnitude of RL between predicted and measured results of 30 mm dia helix may be attributed to significant ohmic impedance compared with input radiation resistance of the antenna and reflection from nearby objects as S parameter measurement was carried out in the lab. The shift in resonance frequency between measured and simulated result is because of the fact that measurements were done using dielectric support structure, whereas simulations were carried out without support structure. This has lowered the measured resonant frequency.

The simulated and measured normalized radiation pattern and phase difference (at resonance frequency) between horizontal and vertical fields for two different helices (dia = 30 mm and 80 mm) at turn angles where these achieve near perfect CP [Figure 3] have been shown in Figures 9 and 10. The measurements were carried out

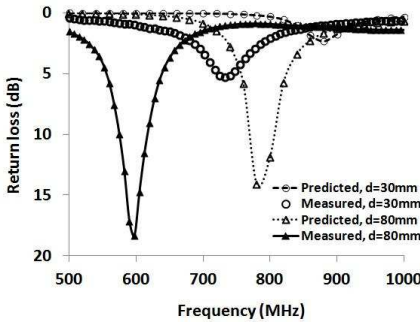


Figure 8. Measured and simulated return loss of helix antennas.

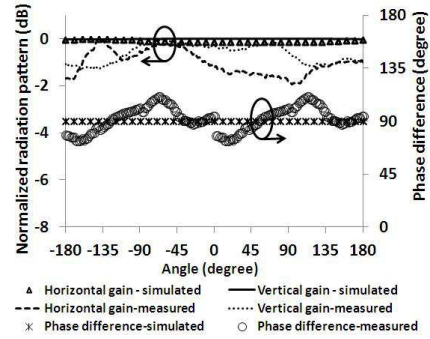


Figure 9. Measured and simulated relative power plots for $d = 30\text{ mm}$ helix in azimuth plane.

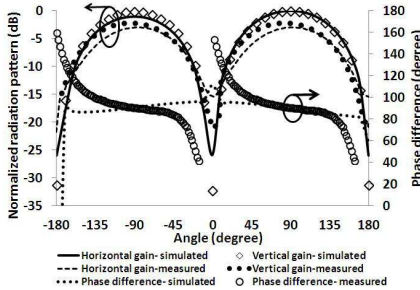


Figure 10. Measured and simulated relative power plots for $d = 80\text{ mm}$ helix in elevation plane.

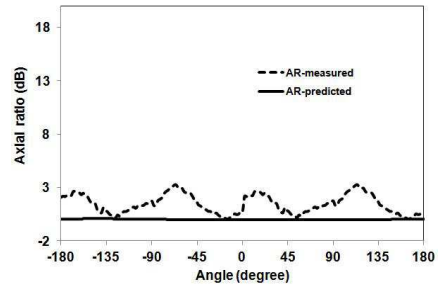


Figure 11. Measured and simulated axial ratio variations for $d = 30\text{ mm}$ helix in azimuth plane.

in anechoic chamber using diamond engineering measurement studio 5.999 H. Figure 9 shows the radiation pattern in azimuth plane for helix of dia 30 mm while Figure 10 depicts the radiation pattern of helix of dia 80 mm in elevation plane. As depicted from Figures 9 and 10, measured and simulated radiation pattern and phase difference (between horizontal and vertical fields) of both antennas within $\text{AR} \leq 3\text{ dB}$ range are in fairly good agreement in both azimuth and elevation plane respectively. The simulated phase difference between vertical and horizontal fields for dia 30 mm helix [Figure 9] is around 90° where as measured phase difference varies in the range of 80° – 110° .

The axial ratio plot of helix with diameter 30 mm is shown in Figure 11 which depicts that simulated axial ratio as 0 dB and measured $\text{AR} \leq 3\text{ dB}$ throughout the azimuth range. Variation in

measured AR for dia 30 mm helix is because of the imbalance in phase [Figure 9] and amplitude of measured signal due to feed discontinuity and various capacitive and inductive effects. Similarly Figure 12 shows comparison of predicted and measured axial ratios for $d = 80$ mm. The predicted axial ratio of the antenna is less than or equal to 2 dB throughout the elevation range whereas the measured axial ratio is less than or equal to 3 dB in 68% of the elevation range. This measured performance is better than the simulated performance of the cross dipole.

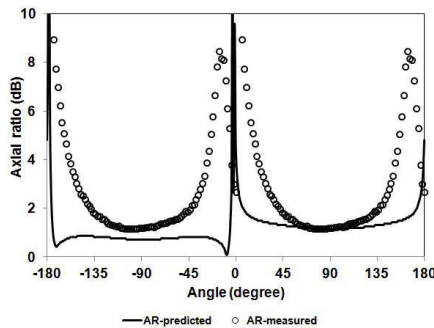


Figure 12. Measured and simulated axial ratio variations for $d = 80$ mm helix in elevation plane.

7. CONCLUSION

This paper presents the design and analysis of CP omnidirectional SFBHAs for different d/L_{hel} ratios. It has been shown that CP SFBHAs can be designed using the equation $A = \rho l$ by Wheeler to obtain wide axial ratio beamwidth for $AR \leq 3$ dB through most of azimuth and elevation range. These antennas are of lowest profile (0.03λ to 0.1λ) in the class of CP omnidirectional antennas not requiring ground plane. The value of turn angle at which near perfect CP is achieved is inversely proportional to the radius of helix and its AR is less sensitive to the variation in turn angle.

REFERENCES

1. Yousaf, J., M. Amin, and S. Iqbal, "Circularly polarized wide axial ratio beamwidth omnidirectional bifilar helix antennas," *Proc. IEEE First AESS European Conf. on Satellite Telecommunication*, 1–6, Oct. 2012.

2. Row, J.-S. and M.-C. Chan, "Reconfigurable circularly-polarized patch antenna with conical beam," *IEEE Trans. on Antennas and Propag.*, Vol. 58, No. 8, 2753–2757, Aug. 2010.
3. Row, J.-S. and K.-W. Lin, "Low-profile design of dual-frequency and dual-polarised triangular microstrip antennas," *Electron. Lett.*, Vol. 40, No. 3, 156–157, Feb. 2004.
4. Iwasaki, H., "A circularly polarized rectangular microstrip antenna using single-fed proximity-coupled method," *IEEE Trans. on Antennas and Propag.*, Vol. 43, No. 8, 895–897, Aug. 1995.
5. Yang, R., R. Mittra, and M. Itoh, "A new omnidirectional CP patch antenna," *Proc. Int. Symp. on Antennas and Propagation, AP-S Digest*, Vol. 3, 1848–1851, Jun. 1994.
6. Iqbal, S., M. Amin, and J. Yousaf, "Designing omnidirectional bifilar helix antenna for circular polarization," *Proc. IEEE First AESS European Conf. on Satellite Telecommunication*, 1–6, Oct. 2012.
7. Iqbal, S., M. Amin, and J. Yousaf, "Low profile circularly polarized side-fed bifilar helix antenna," *Proc. IEEE 9th Int. Bhurban Conf. on Applied Sciences and Technology*, 325–328, Jan. 2012.
8. Leung, K. W., W. C. Wong, and H. K. Ng, "Circularly polarized slot-coupled dielectric resonator antenna with a parasitic patch," *IEEE Antennas Wireless Propag. Lett.*, Vol. 1, No. 1, 57–59, 2002.
9. Chang, F.-S., K.-L. Wong, and T.-W. Chiou, "Low cost broadband circularly polarized patch antenna," *IEEE Trans. on Antennas and Propag.*, Vol. 51, No. 10, 3006–3009, Oct. 2003.
10. Huang, K.-C. and Z. Wang, "Millimeter-wave circular polarized beam-steering antenna array for gigabit wireless communications," *IEEE Trans. on Antennas and Propag.*, Vol. 54, No. 2, 743–746, Feb. 2006.
11. Rappaport, T. S., J. C. Liberti, K. L. Blackard, and B. Tuch, "The effects of antenna gains and polarization on multipath delay spread and path loss at 918 MHz on cross-campus radio links," *Proc. IEEE 42nd Vehicular Technology Conf.*, 550–555, May 1992.
12. Xidong, W., G. V. Eleftheriades, and E. V. Deventer, "Design and characterization of single and multiple beam MM-wave circularly polarized substrate lens antennas for wireless communications," *Proc. Int. Symp. on Antenna and Propagation Society*, Vol. 4, 2408–2412, Aug. 1999.
13. Ryu, K. S. and A. A. Kishk, "UWB dielectric resonator antenna having consistent omnidirectional pattern and low

- crosspolarization characteristics,” *IEEE Trans. on Antennas and Propag.* Vol. 59, No. 4, 1403–1408, Apr. 2011.
14. Sichak, W. and S. Milazzo, “Antennas for circular polarization,” *Proc. IRE*, 997–1001, Aug. 1948.
 15. Solosko, R. B. and S. R. Laxpati, “A log-periodic antenna with vertically polarized omnidirectional radiation,” *IEEE Trans. on Antennas and Propag.*, Vol. 16, No. 6, 752–753, Nov. 1968.
 16. Lin, C.-C., L.-C. Kuo, and H.-R. Chuangl, “A horizontally polarized omnidirectional printed antenna for WLAN applications,” *IEEE Trans. on Antennas and Propag.*, Vol. 54, No. 11, 3551–3556, Nov. 2006.
 17. Hong, W. and K. Sarabandi, “Low profile miniaturized planar antenna with omnidirectional vertically polarized radiation,” *IEEE Trans. on Antennas and Propag.*, Vol. 56, No. 6, 1533–1540, Jun. 2008.
 18. Oh, J. and K. Sarabandi, “A novel high gain low profile miniaturized vertically polarized antenna,” *Proc. Int. Symp. on Antennas and Propagation*, 1–4, Jul. 2010.
 19. Wong, K.-L. and C.-H. Wu, “Wide-band omnidirectional square cylindrical metal-plate monopole antenna,” *IEEE Trans. on Antennas and Propag.*, Vol. 53, No. 8, 2758–2761, Aug. 2005.
 20. Herscovici, N., Z. Sipus, and P.-S. Kildal, “The cylindrical omnidirectional patch antenna,” *IEEE Trans. on Antennas and Propag.*, Vol. 49, No. 12, 1746–1753, Dec. 2001.
 21. Nakano, H., N. Suzuki, T. Ishii, and J. Yamauchi, “Mesh antennas for dual polarization,” *IEEE Trans. on Antennas and Propag.*, Vol. 49, No. 5, 715–723, May 2001.
 22. Iwasaki, H. and N. Chiba, “Circularly polarised back-to-back microstrip antenna with an omnidirectional pattern,” *Proc. IEE Microw. Antennas Propag.*, Vol. 146, No. 4, 277–281, Aug. 1999.
 23. Kawakami, H., G. Sato, and R. Wakabayashi, “Research on circularly polarized conical-beam antennas,” *IEEE Antennas and Propag. Magaz.*, Vol. 39, No. 3, 27–39, Jun. 1997.
 24. Galindo, V. and K. Green, “A near-isotropic circularly polarized antenna for space vehicles,” *IEEE Trans. on Antennas and Propag.*, Vol. 18, No. 6, 872–877, Nov. 1965.
 25. Wang, C.-J. and C.-H. Lin, “A circularly polarized quasi-loop antenna,” *Progress In Electromagnetics Research*, Vol. 84, 333–348, 2008.
 26. Amin, M., J. Yousaf, and M. K. Amin, “Terrestrial mode quadrifilar helix antenna,” *Progress In Electromagnetics Research*

- Letters*, Vol. 27, 179–187, 2011.
27. Dyson, J. D. and P. E. Mayes, “New circularly-polarized frequency-independent antennas with conical beam or omnidirectional patterns,” *IRE Trans. on Antennas Propag.*, 334–342, Jul. 1961.
 28. Amin, M. and R. Cahill, “Effect of helix turn angle on the performance of half wavelength quadrifilar helix antenna,” *IEEE Microw. Wireless Compon. Lett.*, Vol. 16, No. 6, 384–386, Jun. 2006.
 29. Tseng, H.-W. and B. A. Munk, “The generation of omnidirectional circularly polarized far field by a pair of orthogonally oriented vee dipoles,” *Proc. Int. Symp. on Antennas and Propagation, AP-S Digest*, 1042–1045, Jul. 1993.
 30. Amin, M., R. Cahill, and V. Fusco, “Single feed low profile omnidirectional antenna with slant 450 linear polarization,” *IEEE Trans. on Antennas and Propag.*, Vol. 55, No. 11, 3087–3090, Nov. 2007.
 31. Wheeler, H. A., “A helical antenna for circular polarization,” *Proc. IRE*, 1484–1488, Dec. 1947.
 32. Nec-win Professional (Version 1.6), [Online]. Available: Nittany Scientific, 2003.
 33. Ando, A., N. Kita, W. Yamada, K. Itokawa, and A. Sato, “Study of dual-polarized omnidirectional antennas for 5.2 GHz-band 2×2 MIMO-OFDM systems,” *Proc. Int. Symp. on Antennas and Propagation*, Vol. 2, 1740–1743, Jun. 2004.
 34. Li, R.-L. and V. F. Fusco, “Circularly polarized twisted loop antenna,” *IEEE Trans. on Antennas and Propag.*, Vol. 50, No. 10, 1377–1381, Oct. 2002.
 35. Atta, L. C. V., R. J. Mailloux, and M. M. Levenson, “A simple antenna with good circular polarization,” *IEEE Trans. on Antennas and Propag.*, Vol. 17, No. 3, 360–361, May 1969.
 36. Balanis, C. A., *Antenna Theory, Analysis and Design*, 3rd edition, John Wiley and Sons, New York, 2005.
 37. Lee, E.-A., “A low cross-polarization circularly polarized spacecraft TC&R antenna,” *Proc. Int. Symp. on Antennas and Propagation, AP-S Digest*, Vol. 2, 914–917, Jun. 1994.
 38. Huwhrey, L. C., “Characteristic ionospheric multipath phase fluctuations,” *IEEE Trans. on Antennas and Propag.*, 299–300, Mar. 1971.